Mitteilungen

Gesellschaft für Angewandte
Mathematik und Mechanik

Herausgeber
P. Steinmann, Erlangen-Nürnberg

www.gamm-mitteilungen.org

GAMM-Mitt. **37**, No. 1, 124 – 150 (2014) / **DOI** 10.1002/gamm.201410006

Impact and penetration resistance of network models of coated lightweight fabric shielding

T. I. Zohdi*

Department of Mechanical Engineering,
University of California,
Berkeley, CA, 94720-1740, USA

Received 1 August 2013
Published online 7 July 2014

Key words ballistic fabric, shields, lightweight, coating

There exist a wide range of applications for lightweight ballistic fabric shields, such as the protection of critical structural components in transport systems and the human body. However, some deficiencies are (1) the susceptibility to being abruptly severed by sharp objects, which completely eliminates the fabric's ability to stretch and absorb incoming kinetic energy and (2) environmental degradation of the fabric due to moisture, heat and sunlight, which is of growing concern, since many new fabrics have multiple purposes, such as electrical and chemical sensing, in addition to being part of a protective system. Because of these issues, the coating of fabric can be advantageous, however, it adds weight to the shielding system. Experiments on this type of coated fabric system are extremely time-consuming. Accordingly, this paper seeks to develop a computational framework using a coated network model in order to capture the basic characteristics of such systems. One aspect of the model's usefulness is that it can provide qualitative information to guide and reduce costly, time-consuming experiments. Three-dimensional numerical examples are given to illustrate the computational model.

1 Introduction

Multilayered ballistic fabric has become a mainstay of many lightweight commercial and military shielding systems. Unfortunately, there are some weaknesses of fabric shielding, such as the deterioration of the fabric due to environmental exposure and the possibility of being abruptly severed by sharp edges of shrapnel, which destroys the fabric's ability to stretch and absorb incoming objects' kinetic energy. One way to mitigate these problems is to coat the fabric. Explicitly, the advantages of coatings are:

- To help blunt incoming sharp fragments,
- To mitigate the well-known environmental degradation of the polymer-based fabric (such as Zylon, Kevlar and other materials in the aramid-family) and
- To reduce stress concentrations that arise due to abrupt changes in the material properties (fabric-to-metal and vice versa) can be alleviated, by matching the coating properties to

* T. I. Zohdi: e-mail: zohdi@me.berkeley.edu, Phone: +1 510 642 9172

the properties of the other nonfabric layers in the system, for better bonding. In other words, a coated fabric material can be easily bonded to other structures or tailored to have a smooth transition to any other type of layer.

However, a disadvantage of coating a fabric is that it adds weight to the overall system. In the paper we first investigate the trade-offs between increased ballistic resistance and added mass with a mathematical model. One aspect of the model's usefulness is that it can guide and reduce the number of expensive, time-consuming experiments needed (described in the next section) during the development of new types of shields. Furthermore, it serves as a building block in a computational framework for a network model that is constructed later in the paper.

Remark: An issue of increasing concern is protection of fabric-based composite material from environmental exposure, since many new fabrics have multiple purposes, such as electrical and chemical sensing, in addition to being part of a shielding system (Zohdi [48]).[1]

2 Description of experiments

Fig. 1 (online colour at: www.gamm-mitteilungen.org) LEFT: A schematic of the impact scenario. MIDDLE: UC Berkeley facilities Pneumatic gun-breech and barrel set up (top right, photo courtesy of D. Powell). Post impact puncture of Zylon target. *Inset*: The yarn comprising Zylon.

The base structural fabric materials that we are seeking to modify by coating are variants of Zylon (and in some cases Kevlar). Over the last decade, experiments conducted at our laboratory at UC Berkeley have attempted to ascertain the number of sheets of Zylon needed to stop projectiles (Figure 1). *We have no experimental data on coated fabric.* [2] *This experimental work is ongoing, and is extremely costly and time-consuming.* Generally, the microstructure of the fabric fibers is composed of several microscale fibrils. For example, fabric materials such as Zylon, which is a polymeric material constructed from woven PBO (Polybenzoxale) yarn, produced by the Toyobo Corporation (Toyobo [37]), Kevlar and other aramid-based materials have a microstructure comprised of bundles of microscale "microfibrils" forming the fibers, which is then tightly woven into sheets. For Zylon, each fiber contains approximately 350 microfibrils (Figure 1). In order to illustrate the time-consuming complexity of such experiments, *independent of the time needed to coat fabric, which can be signficant,* a

[1] An in depth mathematical analysis of coupled thermal, diffusive and chemical effects in related materials has been conducted by Markenscoff [17-19].

[2] Reports on uncoated fabric, accessible to the public, can be obtained by making a request to the United States Federal Aviation Administration (FAA) indicating project 01-C-AW-WISU. For further experiments on individual yarn, see Verzemnieks [38].

few comments are necessary on the testing processes for the fabric material, conducted at our lab in UC Berkeley (the Werner Goldsmith Ballistics Laboratory). The typical amount of time taken for a single (labor intensive) ballistic test is rather lengthy, on the order of 90 minutes, and is described in detail in Kwong and Goldsmith [16], Zohdi [40], Zohdi and Powell [44], Powell et al. [31], Powell and Zohdi [32] and Powell and Zohdi [33].

To perform the experiments, ballistic sheets of Zylon must be cut with a pair of special scissors from a fabric roll, clamped around a circular bar and placed into a square holder. The two parts of this square frame, whose outside dimensions are 356 mm with a 254 mm square window, are secured by 9.5 mm diameter hard steel bolts via an aluminum strip, which acts as a continuous washer. After these components are assembled, this device is clamped vertically to a heavy triangular support, which is mounted onto a 700 kg steel table so that impact is produced at a preselected location on the target, as specified by a laser beam mounted on the gun centerline. The tests are conducted inside an enclosed room which is evacuated during firing. The initial velocity of the projectile is determined from the time required to successively break two parallel laser beams, 156 mm apart, which were focused on two photodiodes, located 1.5 m in front of the target. The signals from the diodes initiate the start and stop modes of a Hewlett-Packard 5316 time interval meter. Final velocities are determined in three ways: (1) by the use of a digital video recording camera, operating at 10,000 frames/s, that capture the projectile position at a number of instances after the perforation using the dimensions of the projectile, (2) by means of two silver coated paper make-circuit grids spaced 50.4 mm apart, whose voltage pulses are directed to a time interval meter and (3) from two sets of 432×254 mm foils, with each pair separated by 12 mm and each set a distance of 12.7 mm apart, with the projectile contact providing an "on" circuit for each set, allowing the respective signals to start and stop a time interval meter. The number of desired sheets are cut and inserted in the target holder and the bolts were tightened with a 306 N-m torque wrench. The tests were conducted using a custom built gas gun (12.9 mm inside diameter), housed at UC Berkeley in the Werner Goldsmith Ballistics Laboratory, with a 20 mm thick high strength steel barrel of 1.6 m length (see Figure 1). This apparatus is mounted by means of a rail frame onto the same table as the target. A blast shield is placed in front of the muzzle to prevent interaction of ejected debris with the target. A projectile and fragment catcher, consisting of a large cloth filled container, is positioned beyond all final velocity measuring units. [3] The main objective of this work is to develop a relatively simple computational model that captures the main physical features, in order to reduce and guide such time-consuming experiments, which are needed in the development and testing of *new coated fabric systems*. The importance of the computational tool is that it can allow one to probe into the failure mechanisms of the fabric that are not available from our testing facilities.

[3] More information on the experimental setup at UC Berkeley can be found here http: // www.me.berkeley.edu / compmat/ballistics / gasgun.html.

3 Computational framework a network model

3.1 Overall description of the framework

As a starting point, we consider a network of coated yarn that captures (1) stretching of interconnected yarn networks with coating contributions and (2) interaction with impacting projectiles, incorporating contact with friction employing network models (Figure 2). The deformation of the fabric is dictated by solving the coupled system of differential equations for the motion of lumped masses, which are coupled through the fiber-segments under the action of contact forces acting on the network model. We also consider the effects of progressive fiber and coating plastic flow, damage and rupture during the deformation process. The fabric and coating are coupled kinematically, thus leading to a system of differential equations for the deformation of the coated fabric, the rate equations for the inelastic response of the coupled fibers and coating, and the projectile which drives the system through contact. A temporally-adaptive, recursive, staggering scheme is developed to solve this strongly coupled system of equations. Three-dimensional numerical examples are given to illustrate the model

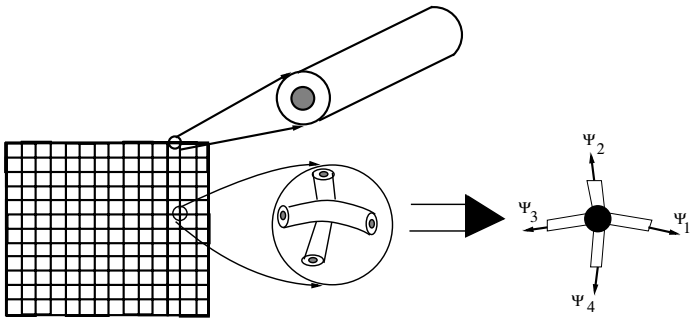

Fig. 2 A patch of coated fabric represented by network model of woven-fabric using coupled fiber-segments. The fiber-segments are joined together by "pin-joint-like" connectors to form a network, whereby sets of equations must be solved for the system dynamics.

3.2 Dynamics of a network model of fabric

The dynamics of the lumped masses are given by

$$m_i\ddot{\boldsymbol{r}}_i = \underbrace{\boldsymbol{\Psi}_i^{tot}}_{total} = \underbrace{\boldsymbol{\Psi}_i^{con}}_{\text{contact forces}} + \underbrace{\sum_{I=1}^{4} \boldsymbol{\Psi}_{I_i}^{yarn}}_{\text{surrounding yarn}} + \underbrace{\sum_{I=1}^{4} \boldsymbol{\Psi}_{I_i}^{coating}}_{\text{surrounding coating}} \tag{1}$$

where $i = 1, 2, ..., N$, where N is the number of lumped masses, $\boldsymbol{\Psi}_{I_i}^{yarn}$ represents the contributions of the four yarns intersecting at mass i, $\boldsymbol{\Psi}_{I_i}^{coating}$ represents the contributions of the four coatings intersecting at mass i and m_i is the mass of a single lumped mass (the total fabric mass divided by the total number of masses). The forces from the Ith surrounding yarn-segment (there are four of them for the type of rectangular weaving pattern considered)

acting on the ith lumped mass is $\boldsymbol{\Psi}_{I_i}^{yarn}$. Clearly, $\boldsymbol{\Psi}_{I_i}^{yarn}$ is a function of the mass positions ($\boldsymbol{r}_i$), which are all coupled together, leading to a system of equations. In order to solve the resulting coupled system, we develop an iterative solution scheme later in the presentation.

3.3 Yarn-segment network representation for mechanical forces

For the network model, we assume that: (1) the yarn-segments are quite thin, experiencing a uniaxial-stress condition, whereby the forces only act along the length of the yarn-segments, (2) the yarn-segments remain straight, undergoing a homogeneous (axial) stress state, (3) the compressive response of a yarn-segment is insignificant (relative to tensile states) and (4) yarn-segment buckling phenomena is ignored. We write one-dimensional constitutive laws in terms of the Piola-Kirchhoff stresses (mimicking 3-D approaches), defined by

$$P = \frac{\text{force on referential area}}{\text{referential area}}, \tag{2}$$

and then transform the result to the the second Piola-Kirchhoff stress via $P = US$, where $U = \frac{L}{L_o}$ is the stretch ratio, L is the deformed length of the yarn-segment, L_o is its original length and where we note that for a relaxed model, when $U \leq 1$ (compression), we enforce $P = 0$. A standard constitutive relation $S = \mathcal{F}(U)$ is then employed, with the primary objective being to extract the force carried in the yarn-segment ($\boldsymbol{\Psi}^{yarn}$), which is needed later for the dynamics of the lumped masses. Specifically,

$$P = \frac{\psi^{yarn}}{A_o} \Rightarrow \psi^{yarn} = USA_o = \frac{L}{L_o} SA_o. \tag{3}$$

We shall adopt a simple one-dimensional model for the stored energy, $W = \frac{1}{2}\mathbb{E}E^2$, where $\mathbb{E}$ is Young's modulus and $E \stackrel{\text{def}}{=} \frac{1}{2}(U^2 - 1)$ is the Green-Lagrange strain, with the second Piola-Kirchhoff stress given by $\frac{\partial W}{\partial E} = S = \mathbb{E}E$. Thus, for the yarn-segment,

$$P = \frac{\psi^{yarn}}{A_o} \Rightarrow \psi^{yarn} = USA_o = \frac{L}{L_o} SA_o = \frac{L}{2L_o}\mathbb{E}\left((\frac{L}{L_o})^2 - 1\right) A_o. \tag{4}$$

Remark 1: As a result of the previous analysis, $\boldsymbol{\Psi}_{I_i}^{yarn} = U_I S_I A_o \boldsymbol{a}_{I_i}$ (A_o is the undeformed cross-sectional area of the yarn), where the unit axial yarn direction is given by $\boldsymbol{a}_{I_i} = \frac{\boldsymbol{r}_I^+ - \boldsymbol{r}_I^-}{||\boldsymbol{r}_I^+ - \boldsymbol{r}_I^-||}$, where $\boldsymbol{r}_I^+$ denotes the position vector of the endpoint connected to the lumped mass and $\boldsymbol{r}_I^-$ denotes the endpoint that is connected to it neighboring mass. [4]

Remark 2: Assumption (3) in the previous section is the adoption of a relaxed-type model, *whereby a zero stress state is enforced for a compressive state.* Relaxed models have a long history, and we refer the reader to works dating back to Pipkin [29], Buchholdt et. al [3], Pangiotopoulos [27], Bufler and Nguyen-Tuong [4], Papadrakakis [28], Cannarozzi [5], [6], Steigmann [34], Haseganu and Steigmann [9-11] and Atai and Steigmann [1, 2]. Relaxed formulations have served as a foundation for computational models describing rupture of

[4] $||\cdot||$ indicates the Euclidean norm in R^3.

ballistic fabric shielding in Zohdi [40], Zohdi and Powell [44] and Powell and Zohdi [32] and are the basis for the present approach.

Remark 3: Consistent with the assumed one-dimensional deformation of the yarn-segments, we have the following relations, between the defomed and undeformed states for the yarn-segment length ($U_I(t) = \frac{L_I(t)}{L_I(t=0)}$), cross-sectional area and volume:

$$\frac{V_I(t)}{V_I(t=0)} = \frac{A_I(t)L_I(t)}{A_I(t=0)L_I(t=0)} = U_I(t), \tag{5}$$

which renders $V_I(t) = V_I(t=0)U(t)$ and $A_I(t) = A_I(t=0)$ (the cross-sectional area remains constant). For other alternative possibilities for one-dimensional yarn responses see Zohdi and Steigmann [41].

3.4 Response of a composite strand

A simple estimate of the increase in stiffness due to the coating can be determined by summing the forces,

$$\sum_{i=1}^{2} \psi_i = \sum_{i=1}^{2} P_i A_{oi} = P_y A_{oy} + P_{co} A_{co} \tag{6}$$

where for the yarns we have from the first Piola-Kirchhoff stress:

$$P_y = \frac{\psi_y}{A_{oy}} \Rightarrow \psi^{yarn} = U^y S^y A_{oy} = \frac{L^y}{L_{oy}} S^y A_{oy} = \frac{L^y}{2L_{oy}} I\!E^y \left((\frac{L^y}{L_{oy}})^2 - 1 \right) A_{oy}. \tag{7}$$

and for the coating

$$P^c = \frac{\psi^c}{A_{oc}} \Rightarrow \psi^{coat} = U^c S^c A_{oc} = \frac{L^c}{L_{oc}} S^c A_{oc} = \frac{L^c}{2L_{oc}} I\!E^c \left((\frac{L^c}{L_{oc}})^2 - 1 \right) A_{oc}. \tag{8}$$

Because of the network model's kinematics, $L^y = L^c = L$, $L_{oy} = L_{oc} = L_o$, $U^y = U^c = U$, one obtains:

$$\psi^y + \psi^c = \frac{L}{2L_o} \left((\frac{L}{L_o})^2 - 1 \right) (I\!E^y A_{oy} + I\!E^c A_{oc}) \,. \tag{9}$$

One can see that the increase in stiffness is directly related to the extensional rigidity $I\!E^c A_{oc}$.

Remark 1: For the coating contribution, the enforcement of zero compressive stress is not necessary. In practice, *for ballistic applications*, the enforcement of this condition makes little difference since the material is nearly always in tension.

Remark 2: In the analysis to follow, the cross-sectional area of the yarn is $A_o^y = \pi R_o^2$ and for the coating of thickness $\mathcal{T}$ it is $A_o^c = \pi((R_o + \mathcal{T})^2 - R_o^2)$. The cross-sectional area

of a Zylon microfibril is $A_o^f = \pi r_f^2$. Thus, effective yarn cross-sectional area in the previous expressions is $A_o^y = 350 \times A_o^f$. This allows us to define the effective yarn radius through

$$\pi R_o^2 = A_o^y = 350 \times A_o^f \Rightarrow R_o = \sqrt{\frac{A_o^y}{\pi}} = \sqrt{\frac{350 \times A_o^f}{\pi}}. \tag{10}$$

We recall that $A_o^c = \pi((R_o + \mathcal{T})^2 - R_o^2)$, which is an effective coating area.

3.5 Damage evolution in a yarn-segment network

Until this point, we have not included yarn damage in the formulation. Generally, the microstructure of the fabric yarn is composed of several microscale fibrils. For example, fabric materials such as Zylon, which is a polymeric material produced by the Toyobo Corporation (Toyobo [37]), Kevlar and other aramid-based materials have a microstructure comprised of bundles of microscale "microfibrils" forming the yarns, which is then tightly woven into sheets. For Zylon, each yarn contains approximately 350 microfibrils, which are randomly misaligned within the yarn, leading to a gradual type of failure, since the microfibrils become stretched to different lengths (within the yarn), when the yarn is in tension. A simple approach (Zohdi and Powell [44]) to describe failure of a yarn is to check whether a critical stretch (for a yarn-segment) has been attained or exceeded, $U(t) \geq U_{crit}$, and to track the progressive damage with a single damage (isotropic) variable, α^y, used construct a new stiffness, $\alpha^y \mathbb{E}^y$, where $0 \leq \alpha^y \leq 1$. The damage variable for each yarn-segment typically has an evolution law associated with it, which represents progressive stretch-induced damage.[5] Specifically, for a yarn that is undamaged, $\alpha^y = 1$, while for a yarn that is completely damaged, $\alpha^y = 0$. For illustration purposes, for example, we adopt the damage representation of Zohdi and Powell [44]

$$\alpha_I^y(t) = min\left(\alpha_I^y(0 \leq t^* < t), e^{(-\lambda(\frac{U_I(t) - U_{I,crit}}{U_{I,crit}}))}\right), \tag{11}$$

where $\alpha_I^y(U_I(t=0)) = 1$, $U_I(t)$ is the stretch of the yarn-segment I at time t, and where $0 \leq \lambda$ is a damage decay parameter. The above relation indicates that damage is irreversible, i.e. α_I^y is a monotonically decreasing function. As $\lambda \to \infty$, the type of failure tends towards sudden rupture, while as $\lambda \to 0$, then there is no damage generated. The progressive damage of yarns can be written for the material constants as, for the Young's modulus, $\mathbb{E}^y(t) = \alpha^y \mathbb{E}^y(t_o)$. Note that as $\alpha^y \to 0$, the physical trends are $\mathbb{E}^y(t) \to 0$. The formulation is repeated for the coating $\mathbb{E}^c(t) = \alpha^c \mathbb{E}^c(t_o)$. The damage variable is relatively easy to track during the staggering scheme. For detailed analysis of damage in materials at the microscale, we refer the reader to Ghosh [7] and Ghosh and Dimiduk [8].

3.6 Plastic flow

In order to incorporate the plastification of the coating and/or yarn, consider the decomposition $F = F_e F_p \Rightarrow U = U_e U_p$, where U_p is sometimes refered to as a "plastic (stretch) strain", and where, if $\sigma \leq \sigma_y$, then $\dot{U}_p = 0$, and if $\sigma > \sigma_y$ and $\sigma > 0$

[5] Multiscale and damage formulations for structural yarns have been explored in detail in Zohdi and Powell [44], Powell and Zohdi [32] and Zohdi [48].

$$\dot{U}_p = \mathcal{P}(\frac{|\sigma|}{\sigma_y} - 1), \tag{12}$$

and if $|\sigma| > \sigma_y$ and $\sigma < 0$

$$\dot{U}_p = -\mathcal{P}(\frac{|\sigma|}{\sigma_y} - 1), \tag{13}$$

where $\mathcal{P}$ is a rate parameter, where σ_y is the yield stress, which has the following stretch sensitivity, $\sigma_y = \sigma_{yo} + \mathcal{H}(U_p)$, where σ_{yo} is the yield stress and $\mathcal{H}(U_p)$ is a hardening variable. Thereafter, one may write $E_e = \frac{1}{2}(U_e^2 - 1)$, and use a simple constitutive law of the form

$$S = I\!\!E E_e = I\!\!E \frac{1}{2}(U_e^2 - 1) = \frac{I\!\!E}{2}((U/U_p)^2 - 1) \tag{14}$$

Remark: Note, one could adopt a different constitutive law using a decomposition of $(E - E_p)$ instead E_e, yielding

$$S = I\!\!E(E - E_p) = I\!\!E(\frac{1}{2}(U^2 - 1) - \frac{1}{2}(U_p^2 - 1)) = \frac{I\!\!E}{2}(U^2 - U_p^2). \tag{15}$$

4 Overall numerical solution scheme

In order describe the overall time-stepping scheme, we first start with the dynamics of a single (ith) lumped mass (Equation 1).

4.1 Adaptive time-stepping scheme

Following Zohdi [44]-[48], employing a trapezoidal-like rule ($0 \leq \phi \leq 1$), we have

$$\frac{\boldsymbol{v}_i(t + \Delta t) - \boldsymbol{v}_i(t)}{\Delta t} = \dot{\boldsymbol{v}}_i(t + \phi \Delta t) \tag{16}$$

and

$$\boldsymbol{v}_i(t + \Delta t) = \boldsymbol{v}_i(t) + \frac{1}{m_i}\int_t^{t+\Delta t} \boldsymbol{\Psi}_i^{tot}\, dt = \boldsymbol{v}_i(t) + \frac{\Delta t}{m_i}\left(\phi \boldsymbol{\Psi}_i^{tot}(t + \Delta t) + (1 - \phi)\boldsymbol{\Psi}_i^{tot}(t)\right). \tag{17}$$

The position can be computed via by applying the mid-point rule again,

$$\boldsymbol{r}_i(t + \Delta t) = \boldsymbol{r}_i(t) + \Delta t \boldsymbol{v}_i(t + \phi \Delta t) \approx \boldsymbol{r}_i(t) + \Delta t\left(\phi \boldsymbol{v}_i(t + \Delta t) + (1 - \phi)\boldsymbol{v}_i(t)\right). \tag{18}$$

By substituting Equation 17 into 18, we obtain

$$\boldsymbol{r}_i(t+\Delta t) = \boldsymbol{r}_i(t)+\boldsymbol{v}_i(t)\Delta t+\frac{\phi(\Delta t)^2}{m_i}\left(\phi \boldsymbol{\Psi}_i^{tot}(\boldsymbol{r}_i(t + \Delta t)) + (1 - \phi)\boldsymbol{\Psi}_i^{tot}(\boldsymbol{r}_i(t))\right)+\hat{\mathcal{O}}(\Delta t)^2, \tag{19}$$

where if $\phi = 1$, then Equation 19 becomes the (implicit) Backward Euler scheme, which is very stable, dissipative and $\hat{\mathcal{O}}(\Delta t)^2 = \mathcal{O}(\Delta t)^2$ locally in time, if $\phi = 0$, then Equation 19 becomes the (explicit) Forward Euler scheme, which is conditionally stable and $\hat{\mathcal{O}}(\Delta t)^2 = \mathcal{O}(\Delta t)^2$ locally in time and if $\phi = 0.5$, then Equation 19 becomes the (implicit) Midpoint scheme, which is stable and $\hat{\mathcal{O}}(\Delta t)^2 = \mathcal{O}(\Delta t)^3$ locally in time. [6] Equation 19 can be solved recursively by recasting the relation as

$$\boldsymbol{r}_i^{L+1,K} = \mathcal{G}(\boldsymbol{r}_i^{L+1,K-1}) + \mathcal{R}_i, \tag{20}$$

where $K = 1, 2, 3, ...$ is the index of iteration within time step $L+1$ and $\mathcal{R}_i$ is a remainder term that does not depend on the solution, i.e. $\mathcal{R}_i \neq \mathcal{R}_i(\boldsymbol{r}_1^{L+1}, \boldsymbol{r}_2^{L+1} ... \boldsymbol{r}_N^{L+1})$. The convergence of such a scheme is dependent on the behavior of $\mathcal{G}$. Namely, a sufficient condition for convergence is that $\mathcal{G}$ is a contraction mapping for all $\boldsymbol{r}_i^{L+1,K}$, $K = 1, 2, 3...$ In order to investigate this further, we define the iteration error as $\varpi_i^{L+1,K} \stackrel{\text{def}}{=} \boldsymbol{r}_i^{L+1,K} - \boldsymbol{r}_i^{L+1}$. A necessary restriction for convergence is iterative self consistency, i.e. the "exact" (discretized) solution must be represented by the scheme

$$\mathcal{G}(\boldsymbol{r}_i^{L+1}) + \mathcal{R}_i = \boldsymbol{r}_i^{L+1}. \tag{21}$$

Enforcing this restriction, a sufficient condition for convergence is the existence of a contraction mapping

$$|| \underbrace{\boldsymbol{r}_i^{L+1,K} - \boldsymbol{r}_i^{L+1}}_{\varpi_i^{L+1,K}} || = ||\mathcal{G}(\boldsymbol{r}_i^{L+1,K-1}) - \mathcal{G}(\boldsymbol{r}_i^{L+1})|| \leq \eta^{L+1,K} ||\boldsymbol{r}_i^{L+1,K-1} - \boldsymbol{r}_i^{L+1}||, \tag{22}$$

where, if $0 \leq \eta^{L+1,K} < 1$ for each iteration K, then $\varpi_i^{L+1,K} \rightarrow \boldsymbol{0}$ for any arbitrary starting value $\boldsymbol{r}_i^{L+1,K=0}$, as $K \rightarrow \infty$. This type of contraction condition is sufficient, but not necessary, for convergence. Explicitly, the recursion is

$$\boldsymbol{r}_i^{L+1,K} = \underbrace{\boldsymbol{r}_i^L + \boldsymbol{v}_i^L \Delta t + \frac{\phi(\Delta t)^2}{m_i} \left((1-\phi) \boldsymbol{\Psi}_i^{tot,L} \right)}_{\mathcal{R}_i} + \underbrace{\frac{\phi(\Delta t)^2}{m_i} \left(\phi \boldsymbol{\Psi}_i^{tot,L+1,K-1} \right)}_{\mathcal{G}(\boldsymbol{r}_i^{L+1,K-1})}, \tag{23}$$

where $\boldsymbol{\Psi}_i^{tot,L+1,K-1} = \boldsymbol{\Psi}_i^{tot,L+1,K-1}(\boldsymbol{r}_1^{L+1,K-1}, \boldsymbol{r}_2^{L+1,K-1} ... \boldsymbol{r}_N^{L+1,K-1})$ and $\boldsymbol{\Psi}_i^{tot,L} = \boldsymbol{\Psi}_i^{tot,L}(\boldsymbol{r}_1^L, \boldsymbol{r}_2^L ... \boldsymbol{r}_N^L)$. The overall objective is to simultaneously maximize the time-step sizes to decrease overall computing time, while obeying an error tolerance on the numerical solution's accuracy. [7] In order to achieve this goal, we follow an approach found in Zohdi [44]-[48], originally developed for continuum thermo-chemical multifield problems where (1) one approximates $\eta^{L+1,K} \approx S(\Delta t)^p$ (S is a constant) and (2) one assumes that the error within an

[6] In order to streamline the notation, we drop the cumbersome $\mathcal{O}(\Delta t)$-type terms.

[7] According to Equation 23, convergence is scaled by $\eta \propto \frac{(\Delta t)^2}{m_i}$, and that the contraction constant of $\mathcal{G}(\boldsymbol{r})$ is (1) directly dependent on the magnitude of the interaction forces, (2) inversely proportional to the lumped masses m_i and (3) directly proportional to Δt. Thus, if convergence is slow within a time step, the time step size, which is adjustable, can be reduced by an appropriate amount to increase the rate of convergence.

iteration to behave according to $(S(\Delta t)^p)^K \varpi^{L+1,0} = \varpi^{L+1,K}$, $K = 1, 2, ...$, where $\varpi^{L+1,0}$ is the initial norm of the iterative error and S is intrinsic to the system. [8] The objective is to meet an error tolerance in exactly a preset number of iterations. To this end, one writes $(S(\Delta t_{\rm tol})^p)^{K_d} \varpi^{L+1,0} = TOL$, where TOL is a tolerance and where K_d is the number of desired iterations. Typically, K_d is chosen to be between five to ten iterations. If the error tolerance is not met in the desired number of iterations, the contraction constant $\eta^{L+1,K}$ is too large. Accordingly, one can solve for a new smaller step size, under the assumption that S is constant, yielding $\Delta t_{\rm tol} = \Delta t \left(\frac{(\frac{TOL}{\varpi^{L+1,0}})^{\frac{1}{pK_d}}}{(\frac{\varpi^{L+1,K}}{\varpi^{L+1,0}})^{\frac{1}{pK}}} \right)$. Numerous parameter studies using this expression can be found in Zohdi [44]-[48]. The assumption that S is constant is not crucial, since the time steps are to be recursively refined and unrefined throughout the simulation.

4.2 Algorithm

(1) GLOBAL FIXED − POINT ITERATION : (SET i = 1 AND K = 0) :
(2) IF i > N THEN GO TO (4) (N = # OF NODES)
(3) IF i ≤ N THEN :
  (a) COMPUTE MASS POSITION : $\boldsymbol{r}_i^{L+1,K}$
  (b) ENFORCE CONTACT IF NECESSARY (DISCUSSED IN NEXT SECTION)
  (c) GO TO (2) AND NEXT MASS (i = i + 1)
(4a) COMPUTE/UPDATE FORCES : $\boldsymbol{\psi}_{\rm i}^{\rm tot,K}$
(4b) COMPUTE/UPDATE FABRIC/COATING DAMAGE : $\alpha_{\rm I}^{\rm y}, \alpha_{\rm I}^{\rm c}$
(4c) COMPUTE/UPDATE FABRIC/COATING PLASTIC STRAIN : $\rm U_{p,I,f}, U_{p,I,c}$
(5) ERROR MEASURE :
  (a) $\varpi_K \stackrel{\rm def}{=} \dfrac{\sum_{i=1}^N ||\boldsymbol{r}_i^{L+1,K} - \boldsymbol{r}_i^{L+1,K-1}||}{\sum_{i=1}^N ||\boldsymbol{r}_i^{L+1,K} - \boldsymbol{r}_i^{L}||}$ (normalized)
  (b) $Z_K \stackrel{\rm def}{=} \dfrac{\varpi_K}{TOL_r}$
  (c) $\Lambda_K \stackrel{\rm def}{=} \left(\dfrac{(\frac{TOL}{\varpi_0})^{\frac{1}{pK_d}}}{(\frac{\varpi_K}{\varpi_0})^{\frac{1}{pK}}} \right)$
(6) IF TOLERANCE MET ($Z_K \leq 1$) AND $K < K_d$ THEN :
  (a) CONSTRUCT NEW TIME STEP : $\Delta t = \Lambda_K \Delta t$
  (b) SELECT MINIMUM : $\Delta t = MIN(\Delta t^{lim}, \Delta t)$
  (c) INCREMENT TIME : $t = t + \Delta t$ AND GO TO (1)
(7) IF TOLERANCE NOT MET ($Z_K > 1$) AND $K = K_d$ THEN :
  (a) CONSTRUCT NEW TIME STEP : $\Delta t = \Lambda_K \Delta t$
  (b) RESTART AT TIME = t AND GO TO (1)

(24)

Remark 1: The expression Λ_K can also be used for time step enlargement (to reduce computational effort) if convergence is met in less than K_d iterations.

Remark 2: External damping (for example from the environment) can easily be incorporated by adding $c_i \dot{\boldsymbol{r}}_i$ in the equations of motion:

$$m_i \ddot{\boldsymbol{r}}_i = \underbrace{\boldsymbol{\Psi}_i^{tot}}_{total} = \underbrace{\boldsymbol{\Psi}_i^{con}}_{\text{contact forces}} + \underbrace{\sum_{I=1}^{4} \boldsymbol{\Psi}_{I_i}^{yarn}}_{\text{surrounding yarn}} + \underbrace{\sum_{I=1}^{4} \boldsymbol{\Psi}_{I_i}^{coating}}_{\text{surrounding coating}} - \underbrace{c_i \dot{\boldsymbol{r}}_i}_{\text{damping}} \tag{25}$$

[8] For the class of problems under consideration, due to the quadratic dependency on Δt, $p \approx 2$.

4.3 Fabric/rigid-body interaction

Following an approach found in Zohdi [46] for rigid projectile-fabric interaction, based on classical contact algorithms, if penetration of a fabric node into the projectile is detected ("contact"), the following process is enacted: (1) Move the fabric node to the closest point on the rigid body's surface.[9] and (2) If there is friction, then a stick condition is assumed (assuming a common position and velocity for the point on the surface of the projectile and the fabric node). The friction force is then checked against the static limit, which if violated, enacts a sliding friction force.

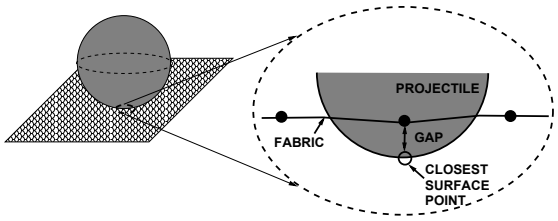

Fig. 3 Interpenetration of a fabric node.

Assuming interpenetration for a node i, we calculate the contact force on a node i (Figure3)

$$\boldsymbol{\psi}_i^{con} = \frac{m_i}{\Delta t^2}(\boldsymbol{r}_i^{f,corr}(t+\Delta t) - \boldsymbol{r}_i^{f,pred}(t+\Delta t)) \tag{26}$$

where the corrected contact position, $\boldsymbol{r}_i^{f,corr}(t+\Delta t)$, is given by

$$\boldsymbol{r}_i^{f,corr}(t+\Delta t) = \boldsymbol{r}_i^{f,pred}(t+\Delta t) + \frac{\Delta t^2}{m_i}\boldsymbol{\psi}_i^{con} \tag{27}$$

and where the predicted contact position, $\boldsymbol{r}_i^{f,pred}(t+\Delta t)$, is given by[10]

$$\boldsymbol{r}_i^{f,pred}(t+\Delta t) = \boldsymbol{r}_i^{f}(t) + \Delta t(\phi \boldsymbol{v}_i^{f,pred}(t+\Delta t) + (1-\phi)\boldsymbol{v}_i^{f}(t)) \tag{28}$$

and

$$\boldsymbol{v}_i^{f,pred}(t+\Delta t) = \boldsymbol{v}_i^{f}(t) + \frac{\Delta t}{m_i}(\phi \boldsymbol{\psi}_i^{f,pred,oth}(t+\Delta t) + (1-\phi)\boldsymbol{\psi}_i^{f,oth}(t)), \tag{29}$$

where $\boldsymbol{\psi}_i^{f,oth}$ are all forces *other* than the contact forces. The fabric node is corrected to

$$\boldsymbol{r}_i^{f,pred}(t+\Delta t) = \boldsymbol{r}_i^{p,cp}(t+\Delta t), \tag{30}$$

[9] There are a variety of algorithms to perform this operation (see Wriggers [39] for details).

[10] $\boldsymbol{v}_i^{f}(t)$ is the converged value from the previous time step.

where $\boldsymbol{r}_i^{p,cp}(t+\Delta t)$ is the closest point on the surface of the contacting object (Figure 3). For an in-depth review of these types of methods see Wriggers [39]. Additionally, we must assign values to the velocity. We first assume that the projectile-fabric surface "sticks". In this case, we assign the velocity of the fabric node to that of the closest point on the body, for node i

$$\boldsymbol{v}_i^{f,corr}(t+\Delta t) = \boldsymbol{v}_i^{p,cp}(t+\Delta t). \tag{31}$$

The friction force is that calculated via

$$\boldsymbol{\psi}_i^{fric} = m_i\dot{\boldsymbol{v}}_i - \boldsymbol{\psi}_i^{con} - \boldsymbol{\psi}_i^{f,oth}. \tag{32}$$

If the friction force exceeds the theoretical limit

$$||\boldsymbol{\psi}_i^{fric}|| > \mu_s||\boldsymbol{\psi}_i^{con}||, \tag{33}$$

then the assumption that there is "stick" is incorrect, and sliding must occur, resulting in a nonmatching velocity of[11]

$$\boldsymbol{v}_i^{f,corr}(t+\Delta t) = \boldsymbol{v}_i^{f,pred}(t+\Delta t) + \frac{\Delta t}{m_i}(\boldsymbol{\psi}_i^{con} + \boldsymbol{\psi}_i^{fric}), \tag{35}$$

with the (frictional) projection

$$\boldsymbol{\psi}_i^{fric} = \mu_d||\boldsymbol{\psi}_i^{con}||\frac{\boldsymbol{v}_i^{p,cp} - \boldsymbol{v}_i^{f,cp}}{||\boldsymbol{v}_i^{p,cp} - \boldsymbol{v}_i^{f,cp}||}. \tag{36}$$

After the calculations culminating with Equation 36 have been completed, the velocity of the projectile is recalculated via (summing the nodal contributions)

$$\boldsymbol{v}^p(t+\Delta t) = \boldsymbol{v}^p(t) - \frac{\Delta t}{m_p}\sum_{i=1}^{N^c}\left(\boldsymbol{\psi}_i^{con} + \boldsymbol{\psi}_i^{fric}\right) + \frac{\Delta t}{m_p}\left(\phi\boldsymbol{\psi}^{p,oth}(t+\Delta t) + (1-\phi)\boldsymbol{\psi}^{p,oth}(t)\right) \tag{37}$$

where N^c is the number of nodes in contact, and

$$\boldsymbol{r}^p(t+\Delta t) = \boldsymbol{r}^p(t) + \Delta t(\phi\boldsymbol{v}^p(t+\Delta t) + (1-\phi)\boldsymbol{v}^p(t)). \tag{38}$$

[11] We remark that the velocity of any point i on the surface of the body can be determined by simply calculating

$$\boldsymbol{v}_i = \boldsymbol{v}_{cm} + \boldsymbol{\omega} \times \boldsymbol{r}_{cm\to i}. \tag{34}$$

The projectile's angular velocity and rotation are determined in a similar manner by integrating the equations for an angular momentum balance

$$\dot{\boldsymbol{H}}_{cm} = \frac{d(\overline{\boldsymbol{I}} \cdot \boldsymbol{\omega})}{dt} = \boldsymbol{M}_{cm}^{EXT}, \tag{39}$$

where $\overline{\boldsymbol{I}}$ is the mass moment of the projectile, $\boldsymbol{\omega}$ is the angular velocity and $\boldsymbol{M}_{cm}^{EXT}$ is the sum of all moment contributions external to the projectile, around its center of mass. A general rigid body solution algorithm is provided in Zohdi [46], as well as in the Appendix.

5 Numerical examples

As an example, we considered a spherical projectile with an incoming velocity of $500\, m/s$, with the following system parameters:

- size of the sheet: $0.254m \times 0.254$ (meters) (=$10in \times 10$ (inches)),
- critical stretch to failure of a Zylon micro-fibril: $U^{*,y} \approx 1.034$ (3 % strain),
- stiffness of a Zylon microfibril: $\mathbb{E}_f = \mathbb{E}^y \approx 180\, GPa$, with a random statistical variation of $\pm$ 10 % from the mean governed by a Gaussian distribution,
- stiffness of the coating: $\mathbb{E}^c = 50\, GPa$,
- radius of a Zylon microfibril: $r_f \approx 5 \times 10^{-6}\, m$,
- density of a Zylon microfibril: $\rho^y \approx 1540\, kg/m^3$ (yarn constructed as before),
- density of the coating: $\rho^c \approx 5000\, kg/m^3$,
- mass of the projectile: $m_p \approx 0.037\, kg$ (spherical) and
- diameter of the spherical projectile: $d \approx 0.025\, m$.
- lumped masses: 100×100 (a 100×100 yarn network weave),
- damage rate for the fabric, $\lambda = 1$ and the plastic rate was zero ($\mathcal{P} = 0$),
- damage rate for the coating, $\lambda = 3$ and the plastic rate was $\mathcal{P} = 1$,
- trapezoidal time-stepping parameter $\phi = 0.5$ (mid-point rule),
- initial (upper limit) time-step size: $\Delta t = 0.000001$ (seconds),
- damping coefficient, $c = 0.01$ (Newton-second/meter),
- iterative tolerance per time step: $TOL = 0.000001$,
- iteration limit per time-step: K_d=6.

Figure 4 shows successive frames taken from the progression of a projectile through multiple sheets. The colors at the nodes indicate the damage (α^y). Generally, one would expect far less sheets would be needed for a smooth blunt projectile (like a sphere) that does not concentrate the force on the fabric yarn. Ongoing work is under way to calibrate the code against ongoing experiments and those conducted over the last few years at the UC Berkeley Ballistics lab (Kwong and Goldsmith [16], Zohdi [40], Zohdi and Powell [44], Zohdi [48], Powell et al [31], Powell and Zohdi [32] and Powell and Zohdi [33]) for various types of projectiles. This example was simply to illustrate the basic construction of the model. Our long-term objective is to fully develop and refine this model to provide information on the failure mechanisms of the *coated yarn*, in particular in the contact zone.

Remark: The trends observed in Figure 4, can be *qualitatively* predicted with simple models, and projectiles with constant contact area, developed in Appendix 2.

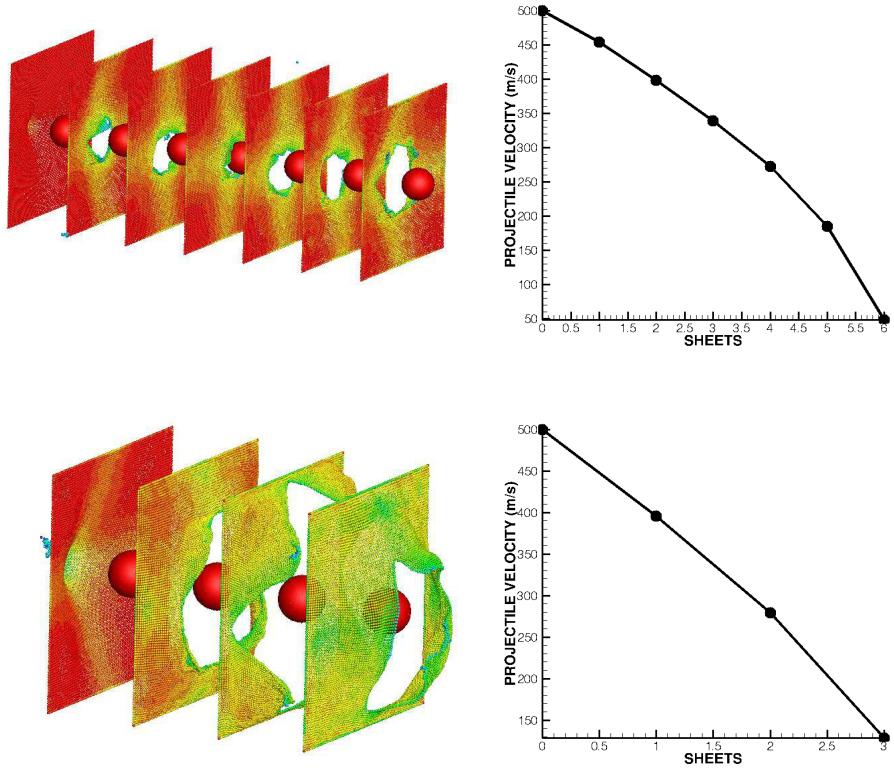

Fig. 4 (online colour at: www.gamm-mitteilungen.org) Incoming velocity (right to left) was $v_o = 500$ m/s. TOP LEFT: For no coating, $\mathcal{T}/R_o = 0$, frames extracted from the progression of a projectile through multiple sheets. The colors indicate the fiber damage (α^y). TOP RIGHT: The velocity in the z-direction as a function of the penetrated sheets. BOTTOM LEFT: For coating, $\mathcal{T}/R_o = 0.25$, $\rho_o = 5000$ kg/m^3, frames extracted from the progression of a projectile through multiple sheets. The colors indicate the fiber damage (α^y). BOTTOM RIGHT: The velocity in the z-direction (initially perpendicular to the sheets) as a function of the penetrated sheets. Statistical randomness was built into the yarn.

6 Extensions and conclusions

In summary, initially, a relation was derived to determine the number of ballistic fabric sheets needed to stop an incoming projectile as a function of the thickness of an added coating. The relation is a function of projectile mass, initial velocity and properties of the yarn and coating (stiffness, stretch to failure, thickness and density). The model served as a basis for a computational tool to study the deformation of coated textiles. In order to simulate such a system, one must solve a set of coupled equations governing the system dynamics. The deformation of the fabric is dictated by solving the coupled system of differential equations for the motion of lumped masses, which are related through the yarn-segments under the action of forces acting on a network model. The quantitative numerical simulations were provided,

using an approach based on a temporally-adaptive staggering time-stepping algorithm. We remark that higher fidelity simulations could be obtained by including other dissipative effects, such as inter-sheet contact, self-contact and friction. However, these effects would appear to be somewhat small for the application under current consideration, since the fabric sheets are quite smooth and combine to produce a low coefficient of friction. However, if the surfaces are rough, or sticky, then intersheet action is quite important. This would require extensive contact search over the fabric surfaces, and efficient techniques for performing this type of calculation are currently being pursued by the author, based on methods of sorting and binning of contact nodes. Methods for fast contact search based on binning of nodes can be found in Pöschel and Schwager [30] and Zohdi [47]. Such approaches assume that a node stays in a certain fixed region (a "bin") for a few time steps, and that one does not need to search over all the other nodes for contact over the whole domain. Furthermore, one can construct so-called "interaction" or "Verlet" lists of neighboring nodes which that node interacts with, for a few time steps, and then update the interaction periodically.

Finally, one critical enhancement to the model are accurate predictions of the effective composite material properties of the coated fabric. Such coating can be produced by particulate spray processing of fabric. There are a number of methods to estimate the overall macroscopic properties of materials particle-functionalized materials, dating back to Maxwell [22], [23] and Lord Rayleigh [26]. For an extensive overview of random heterogeneous media, we refer the reader to Torquato [36], for more mathematical homogenization aspects to Jikov et al.[15], to Hashin [12], Mura [24], Nemat-Nasser and Hori [25], Huet [13], [14] for solid-mechanics oriented works and for computational aspects to Ghosh [7], Ghosh and Dimiduk [8] and Zohdi and Wriggers [45]. Currently, the author is developing methods for spray simulation of fabric, and estimation of the resulting properties, based on a computational models developed in Zohdi [42, 43, 49].

Acknowledgements This work was funded in part by the Army Research Laboratory through the Army High Performance Computing Research Center (cooperative agreement W911NF-07-2-0027) and the Powley foundation.

7 References

1. Atai, A. A. and Steigmann, D. J. (1997). On the nonlinear mechanics of discrete networks. *Archive of Applied Mechanics*. **67**, 303-319.
2. Atai, A. A. and Steigmann, D. J. (1998). Coupled deformations of elastic curves and surfaces. *Int. J. Solids Structures*. **35**, No. 16, 1915-1952.
3. Buchholdt, H. A. Davies, M. Hussey, M. J. L. (1968). The analysis of cable nets. *J. Inst. Maths. Applics.* **4** 339-358.
4. Bufler, H. and Nguyen-Tuong, B. (1980). On the work theorems in nonlinear network theory. *Ing. Arch.* **49** 275-286.
5. Cannarozzi, M. (1987). A minimum principle for tractions in the elastostatics of cable networks. *Int. J. Solids Struct.* **23**, 551-568.
6. Cannarozzi, M. (1985). Stationary and extremum variational formulations for the elastostatics of cable networks. *Meccanica.* **20**, 136-143.
7. Ghosh, S. (2011). Micromechanical Analysis and Multi-Scale Modeling Using the Voronoi Cell Finite Element Method. CRC Press/Taylor & Francis.
8. Ghosh, S. and Dimiduk, D. (2011). Computational Methods for Microstructure-Property Relations. Springer NY.
9. Haseganu, E. M. and Steigmann, D. J. (1994a). Analysis of partly wrinkled membranes by the method of dynamic relaxation.*Computational Mechanics.* **14**, 596-614.

10. Haseganu, E. M. and Steigmann, D. J. (1994b). Theoretical flexural response of a pressurized cylindrical membrane. *Int. J. Solids Struct.* **31**, 27-50.
11. Haseganu, E. M. and Steigmann, D. J. (1996). Equilibrium analysis of finitely deformed elastic networks. *Computational Mechanics.* **17**, 359-373.
12. Hashin, Z. (1983). Analysis of composite materials: a survey. ASME Journal of Applied Mechanics. **50**, 481-505.
13. Huet, C. (1982). Universal conditions for assimilation of a heterogeneous material to an effective medium. Mechanics Research Communications. 9 (3), 165-170.
14. Huet, C. (1984). On the definition and experimental determination of effective constitutive equations for heterogeneous materials. Mechanics Research Communications.**11** (3), 195-200.
15. Jikov, V. V., Kozlov, S. M., Olenik, O. A.(1994). Homogenization of differential operators and integral functionals. Springer-Verlag.
16. Kwong, K. & Goldsmith, W. (2004). Lightweight Ballistic Protection of Flight-Critical Components on Commercial Aircraft - Ballistic Characterization of Zylon. FAA report DOT/FAA/AR-04/45, P1.
17. Markenscoff, X. (2001). Diffusion induced instability. *Quarterly of Applied Mechanics.* Vol. LIX, No. 1, 147-151.
18. Markenscoff, X. (2001). Instabilities of a thermo-mechano-chemical system. *Quarterly of Applied Mechanics.* Vol. LIX, No. 3, 471-477.
19. Markenscoff, X. (2003). On conditions of "negative creep" in amorphous solids. *Mechanics of Materials.* Vol. **35**, Issues 3-6, 553-557.
20. Martin, P. (2009). Handbook of deposition technologies for films and coatings. 3rd Ed. Elsevier.
21. Martin, P. (2011). Introduction to surface engineering and functionally engineered materials. Scrivener and Elsevier.
22. Maxwell, J. C.(1867). On the dynamical theory of gases. Philos. Trans. Soc. London. **157**, 49.
23. Maxwell, J. C. (1873). A treatise on electricity and magnetism. 3rd. Ed. Clarendon Press, Oxford.
24. Mura, T. (1993). Micromechanics of defects in solids, 2nd edition. Kluwer Academic Publishers.
25. Nemat-Nasser, S. and Hori, M. (1999). Micromechanics: overall properties of heterogeneous solids. 2nd edition. Elsevier, Amsterdam.
26. Rayleigh, J. W. (1892). On the influence of obstacles arranged in rectangular order upon properties of a medium. Phil. Mag. **32**, 481-491.
27. Pangiotopoulos, P. D. (1976). A variational inequality approach to the inelastic stress-unilateral analysis of cable structures. *Comput. Struct.* **6** 133-139.
28. Papadrakakis, M. (1980). A method for the automatic evaluation of the dynamic relaxation parameters. *Computer Methods in Applied Mechanics & Engineering.* **25** 35-48.
29. Pipkin, A. C. (1986). The relaxed energy density for isotropic elastic membranes. *IMA Journal of Applied Mathematics.* **36**, 297-308.
30. Pöschel, T. and Schwager, T. 2004. *Computational granular dynamics.* Springer Verlag.
31. Powell, D. Zohdi, T. I. & Johnson, G. (2008). Multiscale Modeling of Structural Fabric Undergoing Impact. FAA report DOT/FAA/AR-08/38.
32. Powell, D. and Zohdi, T. I. (2009). Attachment mode performance of network-modeled ballistic fabric shielding. *Composites Part B: Engineering.* Volume 40, Issue 6, Pages 451-460.
33. Powell, D. and Zohdi, T. I. (2009). A note on flaw-induced integrity reduction of structural fabric. *The International Journal of Fracture/Letters in Micromechanics.* Vol. 158, L89-L96.
34. Steigmann, D. J. (1990). Tension field theory. *Proceedings of the Royal Society London A.* Vol. 429, 141-173.
35. Tabiei, A. & Nilakantan, G. 2008. Ballistic impact of dry woven fabric composites: a review. *Applied Mechanics Reviews.* **61**, 1-13.
36. Torquato, S. (2002). Random Heterogeneous Materials: Microstructure and Macroscopic Properties Springer-Verlag, New York.
37. Toyobo. (2001). PBO fiber ZYLON. Report of the Toyobo Corporation, LTD, www.toyobo.co.jp.
38. Verzemnieks, J. 2005. Lightweight Ballistic Protection of Flight-Critical Components on Commercial Aircraft - Zylon Yarn Tests. FAA report DOT/FAA/AR-05/45, P3.
39. Wriggers, P. 2002. Computational contact mechanics. John-Wiley.
40. Zohdi, T. I. (2002a). Modeling and simulation of progressive penetration of multilayered ballistic fabric shielding. *Computational Mechanics.* **29**, 61-67.
41. Zohdi, T. I. and Steigmann, D. J. (2002b). The toughening effect of microscopic filament misalignment on macroscopic fabric response. *The International Journal of Fracture.* **115**, L9-L14.
42. Zohdi, T. I. (2003). Genetic design of solids possessing a random-particulate microstructure. *Philosophical Transactions of the Royal Society: Mathematical, Physical and Engineering Sciences*. Vol: 361, No: 1806, 1021-1043.

43. Zohdi, T. I. (2004). A computational framework for agglomeration in thermo-chemically reacting granular flows. *Proceedings of the Royal Society.* Vol. 460. Num. 2052, 3421-3445.
44. Zohdi, T. I. and Powell, D. (2006). Multiscale construction and large-scale simulation of structural fabric undergoing ballistic impact. *Computer Methods in Applied Mechanics and Engineering.* Volume 195, Issues 1-3, 94-109.
45. Zohdi, T. I. and Wriggers, P. (2008). Introduction to computational micromechanics. Springer-Verlag.
46. Zohdi, T. I. (2010a) High-speed impact with electromagnetically sensitive fabric and induced projectile spin. *Computational Mechanics*. **46**. 399-415.
47. Zohdi, T. I. (2010b) On the dynamics of charged electromagnetic particulate jets. *Archives of Computational Methods in Engineering*. Volume 17, Number 2, 109-135
48. Zohdi, T. I. (2012). Modeling and simulation of electrification delivery in functionalized textiles in electromagnetic fields. *Computer Methods in Applied Mechanics and Engineering.* Volumes 245246, Pages 206-216.
49. Zohdi, T. I. (2013). Numerical simulation of charged particulate cluster-droplet impact on electrified surfaces. *Journal of Computational Physics.* 233, 509-526.

8 Appendix 1: dynamics of a general rigid body

Following Zohdi [46], since the translational motion of the rigid body has been already considered in the main part of the paper, we now turn to the rotational contribution. There are two, more or less, equivalent approaches to compute the rotations using a (1) Inertially-fixed frame and (2) Body-fixed frame. We employ an inertially-fixed approach for the duration of the presentation.[12] This approach entails, at each (implicit) time step, decomposing an increment of motion into an incremental rigid body translational contribution and an incremental rigid body rotational contribution (rotation about the center of mass). The rotational contribution is determined by solving a set of coupled nonlinear equations governing the angular velocity and the incremental rotation of the body around the axis of rotation (which also changes as a function of time, and must also be determined). The equation for the angular momentum can be written using fixed inertial coordinates

$$\dot{\boldsymbol{H}}_{cm} = \frac{d(\overline{\boldsymbol{I}} \cdot \boldsymbol{\omega})}{dt} = \boldsymbol{M}_{cm}^{EXT}. \tag{40}$$

Because the body rotates, the moment of inertia about the center of mass, $\overline{\boldsymbol{I}}$, is implicitly dependent on $\boldsymbol{\omega}$ (and hence time), which leads to a coupledsystem of nonlinear ODE's, which will be solved with an iterative scheme. Equation 40 is discretized by a trapezoidal scheme

$$\frac{d(\overline{\boldsymbol{I}} \cdot \boldsymbol{\omega})}{dt}|_{t+\phi\Delta t} = \frac{(\overline{\boldsymbol{I}} \cdot \boldsymbol{\omega})|_{t+\Delta t} - (\overline{\boldsymbol{I}} \cdot \boldsymbol{\omega})|_{t}}{\Delta t}. \tag{41}$$

thus leading to

$$(\overline{\boldsymbol{I}} \cdot \boldsymbol{\omega})|_{t+\Delta t} = (\overline{\boldsymbol{I}} \cdot \boldsymbol{\omega})|_{t} + \Delta t \boldsymbol{M}_{cm}^{EXT}(t + \phi\Delta t). \tag{42}$$

Solving for $\boldsymbol{\omega}(t + \Delta t)$ yields

$$\boldsymbol{\omega}(t + \Delta t) = \left(\overline{\boldsymbol{I}}(t + \Delta t)\right)^{-1} \cdot \left((\overline{\boldsymbol{I}} \cdot \boldsymbol{\omega})|_{t} + \Delta t \boldsymbol{M}_{cm}^{EXT}(t + \phi\Delta t) \right), \tag{43}$$

[12] For a body-fixed formulation, see Powell and Zohdi [31].

where

$$\boldsymbol{M}_{cm}^{EXT}(t+\phi\Delta t) \approx \phi \boldsymbol{M}_{cm}^{EXT}(t+\Delta t) + (1-\phi)\boldsymbol{M}_{cm}^{EXT}(t) \tag{44}$$

which yields an implicit nonlinear equation, of the form $\boldsymbol{\omega}(t+\Delta t) = \mathcal{F}(\boldsymbol{\omega}(t+\Delta t))$, since $\overline{\boldsymbol{I}}(t+\Delta t)$, due to the body's rotation. An iterative, implicit, solution scheme may be written as follows for $K = 1, 2...$

$$\boldsymbol{\omega}^{K+1}(t+\Delta t) = \left(\overline{\boldsymbol{I}}^{K}(t+\Delta t)\right)^{-1} \cdot \left((\overline{\boldsymbol{I}} \cdot \boldsymbol{\omega})|_t + \Delta t \boldsymbol{M}_{cm}^{EXT,K}(t+\phi\Delta t)\right), \tag{45}$$

where $\overline{\boldsymbol{I}}^{K}(t+\Delta t)$ can be computed by a similarity transform (described shortly) [13]. After the update for $\boldsymbol{\omega}^{K+1}(t+\Delta t)$ has been computed (utilizing the $\overline{\boldsymbol{I}}^{K}(t+\Delta t)$ from the previous iteration), the rotation of the body about the center of mass can be determined. The *incremental* angular rotation around the instantaneous rotation axis $\boldsymbol{a}^{K+1}(t+\phi\Delta t)$ (which will also have to be updated) is obtained by

$$\frac{d\theta^{K+1}}{dt}(t+\phi\Delta t) = \omega^{K+1}(t+\phi\Delta t) \approx \frac{\Delta\theta^{K+1}(t+\phi\Delta t)}{\Delta t} \tag{46}$$

where $\boldsymbol{\omega}^{K+1}(t+\phi\Delta t) = \omega^{K+1}(t+\phi\Delta t)\boldsymbol{a}^{K+1}(t+\phi\Delta t)$, $\omega^{K+1}(t+\phi\Delta t)$ being *a scalar* rotation about the instantaneous axis,

$$\boldsymbol{a}^{K+1}(t+\phi\Delta t) \stackrel{\text{def}}{=} \frac{\boldsymbol{\omega}^{K+1}(t+\phi\Delta t)}{||\boldsymbol{\omega}^{K+1}(t+\phi\Delta t)||} \approx \frac{\phi\boldsymbol{\omega}^{K+1}(t+\Delta t) + (1-\phi)\boldsymbol{\omega}(t)}{||\phi\boldsymbol{\omega}^{K+1}(t+\Delta t) + (1-\phi)\boldsymbol{\omega}(t)||}, \tag{47}$$

and thus

$$\Delta\theta^{K+1}(t+\phi\Delta t) = \omega^{K+1}(t+\phi\Delta t)\Delta t, \tag{48}$$

where $\omega^{K+1}(t+\Delta t) = ||\phi\boldsymbol{\omega}^{K+1}(t+\Delta t) + (1-\phi)\boldsymbol{\omega}(t)||$. To determine the movement of the individual points on the rigid body, we need to perform a rigid body translation and rotation (described in the next section). For example, consider a point $\boldsymbol{r}_i$ on the body. The update would be

$$\boldsymbol{r}_i(t+\Delta t) = \boldsymbol{r}_i(t) + \underbrace{\boldsymbol{u}_{cm}}_{due\ to\ cm\ translation} + \underbrace{\boldsymbol{u}_{i,rot}}_{due\ to\ rotation\ wrt\ cm} \tag{49}$$

where $\boldsymbol{u}_{cm} = \boldsymbol{r}_{cm}(t+\Delta t) - \boldsymbol{r}_{cm}(t)$ and where $\boldsymbol{u}_{i,rot}$ is contribution due to an incremental rotation of the relative position vector $\boldsymbol{\tau}^{(i)} \stackrel{\text{def}}{=} \boldsymbol{r}_i(t) - \boldsymbol{r}_{cm}(t)$ by $\Delta\theta$ about the cm (Figure 5).

[13] One may view the overall process as a fixed-point calculation of the form $\boldsymbol{\omega}^{K+1}(t+\Delta t) = \mathcal{F}(\boldsymbol{\omega}^{K}(t+\Delta t))$.

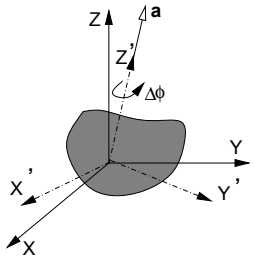

Fig. 5 Aligning the primed coordinate system with the instantaneous axis of rotation (for a general body, Zohdi [46]).

8.1 Transformation matrices for updates and incremental rotation

In order to rotate any point i associated with the rigid body, with position vector $\boldsymbol{\tau}^{(i)}$ we require some standard transformations. The same transformation are needed to rotate the body's moment of inertia, $\overline{\boldsymbol{I}}$. It is a relatively standard exercise in linear algebra to show that any vector, $\boldsymbol{\tau}$, which can be expressed in either the unprimed or primed basis, $\boldsymbol{\tau} = (\boldsymbol{\tau} \cdot \boldsymbol{e}_i)\boldsymbol{e}_i = (\boldsymbol{\tau} \cdot \boldsymbol{e}'_j)\boldsymbol{e}'_j$ where summation index notation is employed. These two representations are explicitly related by

$$\left[\begin{array}{c} \tau_1 \\ \tau_2 \\ \tau_3 \end{array} \right]' = \underbrace{\left[\begin{array}{ccc} \boldsymbol{e}_1 \cdot \boldsymbol{e}'_1 & \boldsymbol{e}_2 \cdot \boldsymbol{e}'_1 & \boldsymbol{e}_3 \cdot \boldsymbol{e}'_1 \\ \boldsymbol{e}_1 \cdot \boldsymbol{e}'_2 & \boldsymbol{e}_2 \cdot \boldsymbol{e}'_2 & \boldsymbol{e}_3 \cdot \boldsymbol{e}'_2 \\ \boldsymbol{e}_1 \cdot \boldsymbol{e}'_3 & \boldsymbol{e}_2 \cdot \boldsymbol{e}'_3 & \boldsymbol{e}_3 \cdot \boldsymbol{e}'_3 \end{array} \right]}_{[\boldsymbol{A}]} \left[\begin{array}{c} \tau_1 \\ \tau_2 \\ \tau_3 \end{array} \right]. \tag{50}$$

Note that $\boldsymbol{A}^{-1} = \boldsymbol{A}^T$, thus $\boldsymbol{\tau}' = \boldsymbol{A} \cdot \boldsymbol{\tau}$ and $\boldsymbol{\tau} = \boldsymbol{A}^T \cdot \boldsymbol{\tau}'$. This basic result can be used to perform rotation of a vector about an axis, as well as the rotation of the inertia tensor. Without any loss of generality, we align the $\boldsymbol{e}'_3$ axis to instantaneous rotation axis $\boldsymbol{a}$. The total transformation (rotation) of a vector $\boldsymbol{\tau}^{(i)}$ representing a point i on the body, can be represented by

$$[\boldsymbol{\tau}^{(i)}]^{rot} = \underbrace{[\boldsymbol{A}]^T \underbrace{[\boldsymbol{R}(\Delta\theta)] \underbrace{[\boldsymbol{A}][\boldsymbol{\tau}_i]}_{[\boldsymbol{\tau}^{(i)}]'}}_{[\boldsymbol{\tau}^{(i)}]^{rot,\prime}}}_{[\boldsymbol{\tau}^{(i)}]^{rot}} \tag{51}$$

where

$$[\boldsymbol{R}(\Delta\theta)] = \left[\begin{array}{ccc} cos(\Delta\theta) & -sin(\Delta\theta) & 0 \\ sin(\Delta\theta) & cos(\Delta\theta) & 0 \\ 0 & 0 & 1 \end{array} \right] \tag{52}$$

Similarly, for the rotation inertia tensor

$$[\overline{\boldsymbol{I}}]^{rot} = [\boldsymbol{A}]\,[\boldsymbol{R}(\Delta\theta)]^T \underbrace{\underbrace{\underbrace{[\boldsymbol{A}]^T[\overline{\boldsymbol{I}}][\boldsymbol{A}]}_{[\overline{\boldsymbol{I}}]'}}_{[\overline{\boldsymbol{I}}]^{rot,\prime}}}_{[\overline{\boldsymbol{I}}]^{rot}}[\boldsymbol{R}(\Delta\theta)][\boldsymbol{A}]^T, \tag{53}$$

where, during the iterative calculations, $[\overline{\boldsymbol{I}}] = [\overline{\boldsymbol{I}}(t)]$ and $[\overline{\boldsymbol{I}}]^{rot} = [\overline{\boldsymbol{I}}(t+\Delta t))]$.

8.2 Algorithmic procedure

The overall procedure is as follows, at time t:

1. Compute the new position of the center of mass.
2. Compute (iteratively) the incremental angular rotation of the body with respect to the center of mass until system convergence:

$$||\boldsymbol{\omega}^{K+1}(t+\Delta t) - \boldsymbol{\omega}^{K}(t+\Delta t)|| \leq TOL||\boldsymbol{\omega}^{K+1}(t+\Delta t)||. \tag{54}$$

   This requires a rotation of the body within the iterations:

   (a) Given that $\boldsymbol{\omega}^{K+1}(t+\Delta t)$ has been computed

$$\boldsymbol{\omega}^{K+1}(t+\Delta t) = \left(\overline{\boldsymbol{I}}^{K}(t+\Delta t)\right)^{-1} \cdot \left((\overline{\boldsymbol{I}}\cdot\boldsymbol{\omega})|_t + \Delta t \boldsymbol{M}_{cm}^{EXT,K}(t+\phi\Delta t)\right) \tag{55}$$

   (b) Compute the (updated) axis of rotation:

$$\boldsymbol{a}^{K+1}(t+\phi\Delta t) \stackrel{\text{def}}{=} \frac{\boldsymbol{\omega}^{K+1}(t+\phi\Delta t)}{||\boldsymbol{\omega}^{K+1}(t+\phi\Delta t)||} \approx \frac{\phi\boldsymbol{\omega}^{K+1}(t+\Delta t) + (1-\phi)\boldsymbol{\omega}(t)}{||\phi\boldsymbol{\omega}^{K+1}(t+\Delta t) + (1-\phi)\boldsymbol{\omega}(t)||}. \tag{56}$$

   (c) Compute the basis $\boldsymbol{e}_3'$-aligned instantaneous axis of rotation:

   (i) $\boldsymbol{e}_3'$, is aligned with $\boldsymbol{a}^{K+1}(t+\Delta t)$

   (ii) $\boldsymbol{e}_1' = \boldsymbol{e}_3' \times \boldsymbol{e}_3/||\boldsymbol{e}_3' \times \boldsymbol{e}_3||$ and

   (iii) $\boldsymbol{e}_2' = \boldsymbol{e}_3' \times \boldsymbol{e}_1'/||\boldsymbol{e}_3' \times \boldsymbol{e}_1'||$

   (d) Compute the composite transformation for the inertia tensor in Equation 53 and obtain the update $\overline{\boldsymbol{I}}^{K+1}(t+\Delta t)$.

   (e) Repeat steps (a)-(d) until Equation 55 is satisfied.
3. Compute the total new position of the points on the body (i) with Equation 51, increment time forward and repeat the procedure.

9 Appendix 2: some analytical modeling

As mentioned in the body of the paper, the trends observed in Figure 4, can be *qualitatively* predicted with simple models, and projectiles with constant contact area, which are described in the following sections.

9.1 Stretching and rupture

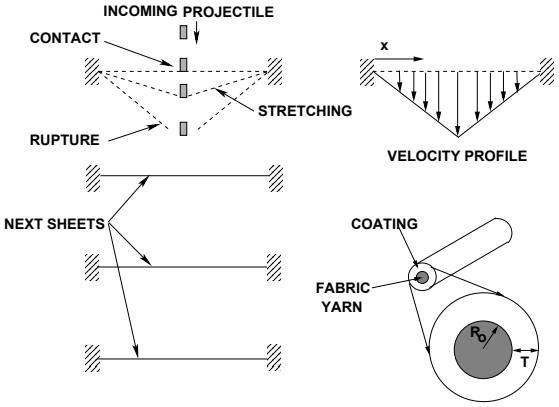

Fig. 6 The idealized sequence of events.

We initially consider the stretching and rupture of a single yarn in the fabric, and later extend the analysis to the response of multiple yarn in a sheet within the projectile contact zone. We denote ρ_o^y as the initial (undeformed) density of the yarn and A_o^y is the initial cross-sectional area. During the stretching to final rupture, the yarn is assumed to attain a linear (symmetric) velocity profile ($0 \leq x \leq L_o/2$) given by $v(x) = v_p 2x/L_o$, where v_p is the velocity of the projectile (Figure 6). We assume that the contact area of the projectile/fabric is sufficiently small with respect to the target size so that it can be considered as a point load during this stage of the analysis. Later, the dimensions of the projectile will be taken into account. By integrating the differential kinetic energy, we obtain

$$2\int_0^{\frac{L_o}{2}} \frac{1}{2}\rho_o^y A_o^y (v(x))^2\, dx = \frac{\rho_o^y A_o^y L_o}{6}(v_p)^2. \tag{57}$$

An energy balance yields

$$\underbrace{\frac{1}{2}m_p(v_p^{(i)})^2}_{\text{kinetic eng. after ith sheet}} - \underbrace{w^y(U^{*,y})}_{\text{absorbed elastic eng.}} = \underbrace{\frac{1}{2}m_p(v_p^{(i+1)})^2}_{\text{kinetic eng. after i+1 th sheet}} + \underbrace{\frac{\rho_o^y A_o^y L_o}{6}(v_p^{(i+1)})^2}_{\text{fabric kinetic eng.}}, \tag{58}$$

where the stretch throughout the yarn (on either side of the projectile) has been approximated as being uniform, due to the assumed linear mode of deformation (Figure 6). The absorbed (stored) energy at failure is denoted $w^y(U^{*,y})$, where $U^{*,y}$ is the critical stretch ratio at failure.

The stretch ratio is defined as $U \stackrel{\text{def}}{=} \frac{L}{L_o}$, where L is the stretched length and L_o is the original unstretched length. Equation 58 may be written in the form of a recursion (i=sheet counter number)

$$v_p^{(i+1)} = \sqrt{\alpha (v_p^{(i)})^2 - \beta}, \tag{59}$$

where

$$\alpha = \frac{m_p}{m_p + \frac{\rho_o^y A_o^y L_o}{3}} \qquad \text{and} \qquad \beta = \frac{2 w^y (U^{*,y})}{m_p + \frac{\rho_o^y A_o^y L_o}{3}}. \tag{60}$$

For moderate finite strains (the case here), the response of the thin one-dimensional yarn can be accurately described by a constitutive law of the form $S = I\!E^y E$, where S is the second Piola-Kirchhoff stress, $I\!E^y$ is the Young's modulus and $E \stackrel{\text{def}}{=} \frac{1}{2}(U^2 - 1)$ is the Green-Lagrange strain. The quantity of interest here is the absorbed (stored) energy $w^y(U^{*,y}) = \frac{L_o A_o^y}{2} I\!E^y (\frac{(U^{*,y})^2 - 1}{2})^2$ at final rupture, where $W^y(U^{*,y}) \stackrel{\text{def}}{=} \frac{1}{2} I\!E^y \left(\frac{(U^{*,y})^2 - 1}{2} \right)^2$ is the absorbed (stored) energy per unit volume. We shall use this simple absorbed (stored) energy function in the analysis that follows. However, we note that other material models could easily be employed without any complication.

Remark 1: The axial strains, for structural fabric such as Zylon or Kevlar, are expected to be in the range of 2 %-10 % before rupturing.[14] Therefore, a relatively simple Kirchhoff-St. Venant material model is reasonable. Although it is not explicitly needed in this analysis, the Cauchy stress (σ) is related to the second Piola-Kirchhoff stress in the following manner for this simple one-dimensional case, $\sigma = US = \sigma = I\!E \frac{U^3 - U}{2}$.

Remark 2: The use of a linear velocity profile was motivated by observations in laboratory experiments and large scale numerical studies for sheets of fabric that are clamped to a target holder (Kwong and Goldsmith [16], Zohdi [40], Zohdi and Powell [44], Powell et al. [31], Powell and Zohdi [32] and Powell and Zohdi [33]).

Remark 3: The exact mechanism for damage evolution and fracture of the fabric is outside the scope of the present work. The reader is referred to the recent work of Ghosh [7] and Ghosh and Dimiduk [8] for a thorough review and analysis of the micromechanisms of damage evolution and failure for a variety of lightweight composite materials.

9.2 Introduction of a coating layer

Now we augment the model with a coating (superscript c) layer (Figure 6) which is assumed to undergo the same loading as the fabric (superscript y), to which it is bonded. Integrating the differential kinetic energy, we obtain

$$2 \left(\int_0^{\frac{L_o}{2}} \frac{1}{2} \rho_o^y A_o^y (v(x))^2 \, dx + \int_0^{\frac{L_o}{2}} \frac{1}{2} \rho_o^c A_o^c (v(x))^2 \, dx \right) = \frac{\rho_o^y A_o^y L_o}{6} (v_p)^2 + \frac{\rho_o^c A_o^c L_o}{6} (v_p)^2. \tag{61}$$

[14] For example, Zylon ruptures at approximately a 3 % axial strain (Toyobo [37]).

An energy balance yields

$$\underbrace{\frac{1}{2}m_p(v_p^{(i)})^2}_{\text{kin. eng. after ith sheet}} - \underbrace{w^y(U^{*,y})}_{\text{absorbed fab. eng.}} - \underbrace{w^c(U^{*,c})}_{\text{absorbed coat. eng.}} = \underbrace{\frac{1}{2}m_p(v_p^{(i+1)})^2}_{\text{kin. eng. after i+1 th sheet}} + \underbrace{\frac{\rho_o^y A_o^y L_o}{6}(v_p^{(i+1)})^2}_{\text{fab. kin. eng.}} + \underbrace{\frac{\rho_o^c A_o^c L_o}{6}(v_p^{(i+1)})^2}_{\text{coat. kin. eng.}}. \quad (62)$$

Equation 62 may be written in the form of a recursion

$$v_p^{(i+1)} = \sqrt{\alpha(v_p^{(i)})^2 - \beta}, \quad (63)$$

where

$$\alpha = \frac{m_p}{m_p + \frac{(\rho_o^y A_o^y + \rho_o^c A_o^c)L_o}{3}} \quad \text{and} \quad \beta = \frac{2(w^y(U^{*,y}) + w^c(U^{*,c}))}{m_p + \frac{(\rho_o^y A_o^y + \rho_o^c A_o^c)L_o}{3}}. \quad (64)$$

For the coating, for illustration purposes, we will assume that it is a metal-like, and ignore the small elastic strains and assume a dissipated amount of plastic work/energy of the form, $w^c(U^{*,c}) = \frac{L_o A_o^c}{2}\mathbb{E}^{c,p}(\frac{(U^{*,c})^2-1}{2})^2$, where $\mathbb{E}^{c,p}$ is the plastic or damaged modulus of the material, and $U^{*,c}$ is the strain to complete failure of the coating.

Remark: The cross-sectional area of the yarn is $A_o^y = \pi R_o^2$ and for the coating of thickness $\mathcal{T}$ it is $A_o^c = \pi((R_o + \mathcal{T})^2 - R_o^2)$.

9.3 Estimation of the number of sheets

Equation 63 can be put into an easier to manipulate form by squaring both sides to obtain

$$(v_p^{(i+1)})^2 = \alpha(v_p^{(i)})^2 - \beta, \quad (65)$$

and subtracting this result from the relation evaluated at the previous sheet

$$(v_p^{(i)})^2 = \alpha(v_p^{(i-1)})^2 - \beta, \quad (66)$$

to yield

$$\frac{(v_p^{(i+1)})^2 - (v_p^{(i)})^2}{(v_p^{(i)})^2 - (v_p^{(i-1)})^2} = \alpha. \quad (67)$$

Thus, the ratio of the loss of kinetic energy, $\frac{1}{2}m_p v_p^2$, from sheet to sheet, is constant, and therefore

$$(v_p^{(i+1)})^2 - (v_p^{(i)})^2 = \alpha^i \left((v_p^{(1)})^2 - (v_p^{(0)})^2\right), \quad (68)$$

where the notation α^i denotes α to the ith power (as opposed to superscript (i)). As a result, we obtain an expression relating the sheets penetrated (i) to the velocities between layers

$$i = \frac{1}{ln\alpha} ln \left(\frac{(v_p^{(i+1)})^2 - (v_p^{(i)})^2}{(v_p^{(1)})^2 - (v_p^{(0)})^2} \right). \tag{69}$$

Setting the velocity at sheet $i+1$ to zero yields an expression for the velocity after i sheets have been penetrated,

$$(v_p^{(i+1)})^2 = \alpha (v_p^{(i)})^2 - \beta = 0 \Rightarrow v_p^{(i)} = \sqrt{\frac{\beta}{\alpha}}. \tag{70}$$

Combining the two previous relations, we obtain the number of sheets (i^*) that a projectile will penetrate before stopping

$$\frac{(0)^2 - \frac{\beta}{\alpha}}{(v_p^{(1)})^2 - (v_p^{(0)})^2} = \alpha^i \Rightarrow i^* = \frac{1}{ln\alpha} ln \left(\frac{-\frac{\beta}{\alpha}}{(v_p^{(1)})^2 - (v_p^{(0)})^2} \right). \tag{71}$$

By applying the recursion relation to the first sheet

$$(v_p^{(1)})^2 = \alpha (v_p^{(0)})^2 - \beta \Rightarrow (v_p^{(1)})^2 - (v_p^{(0)})^2 = \alpha (v_p^{(0)})^2 - \beta - (v_p^{(0)})^2, \tag{72}$$

we obtain an expression for the number of sheets penetrated solely in terms of the system parameters and the initial velocity

$$i^* = \frac{1}{ln\alpha} ln \left(\frac{\frac{-\beta}{\alpha}}{(\alpha - 1)(v_p^{(0)})^2 - \beta} \right). \tag{73}$$

Since i^* represents the number of sheets penetrated, it should be rounded up to an integer value. Furthermore, since $i^* + 1$ represents the number of sheets needed to stop the projectile, it should also be rounded up to an integer value. Rounding the values up will provide a conservative estimate in each case.

9.4 Experimental observations/estimated ballistic resistance

We have some limited tests on uncoated (for the zero-thickness ($\mathcal{T} = 0$) case) materials which we can use to compare the analytical expression (Equation 73) against. In order to do this, we extend the analytical expression to describe a sheet with multiple participating yarn (Figure 7). Typically, for structural fabric, the microstructure of the yarn is composed of groups of microscale fibrils. As mentioned earlier, Zylon (the material that we have extensive data for) possesses such a multiscale structure, constructed from PBO (Polybenzoxale) microscale fibrils, which are bundled to form yarn, which are then tightly woven into sheets Figure 6. The following system parameters (from the described experiments) and standard properties of Zylon fabric (Toyobo [37]) were used:

- length of the target: $L_o \approx 0.254\, m$,
- critical stretch to failure of a Zylon micro-fibril: $U^{*,y} \approx 1.034$ (3 % strain),
- stiffness of a Zylon microfibril: $\mathbb{E}_f = \mathbb{E}^y \approx 180\, GPa$,
- radius of a Zylon microfibril: $r_f \approx 5 \times 10^{-6}\, m$,

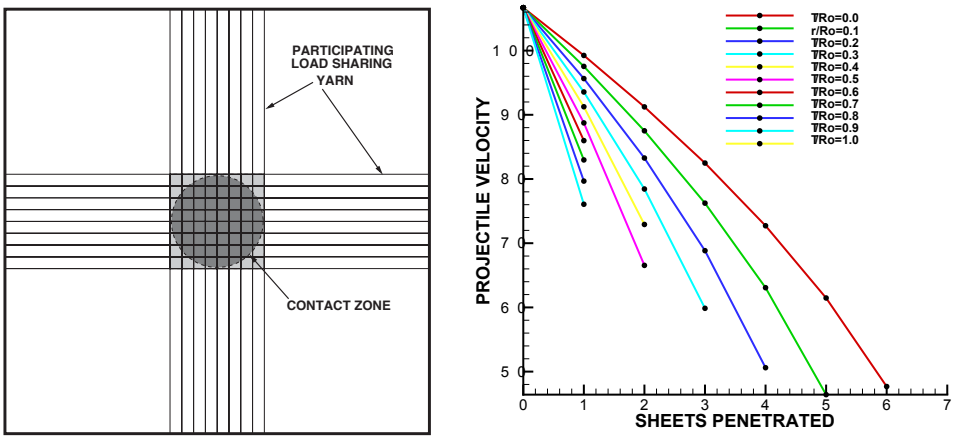

Fig. 7 (online colour at: www.gamm-mitteilungen.org) LEFT: An approximate determination of the total number of load sharing yarn is determined by computing the number of yarn in the horizontal direction in contact region and the number of yarn in the vertical direction. Essentially only the yarn shown participate/contribute to any significant degree in the ballistic resistance for clamped boundary conditions. RIGHT: For $v_o = 106 m/s$ and coating variation of $\mathcal{T}/R_o = 0, 0.1, 0.2...1$, with a coating density of $\rho^c = 5000 kg/m^3$ and stiffness being the same ($I\!E^c/I\!E^y = 1$) as the fabric. For $\mathcal{T}/R_o = 0$ (top curve), approximately $i^* = 6.52$ (rounded up to seven) were predicted penetrated by the theory, and $i^*+1 = 7.52$ (rounded up to eight) were predicted to stop the projectile. This is nearly the exact number indicated by the experiments (six sheets penetrated and seven to stop the projectile).

- density of a Zylon microfibril: $\rho_o \approx 1540\, kg/m^3$,
- mass of the projectile: $m_p \approx 0.036\, kg$ and
- diameter of the projectile cross-section: $d \approx 0.0127\, m$.

The cross-sectional area of a Zylon microfibril is $A_o^f = \pi r_f^2$. Thus, effective yarn cross-sectional area in the previous expressions is $A_o^y = 350 \times A_o^f$. This allows us to define the effective yarn radius through

$$\pi R_o^2 = A_o^y = 350 \times A_o^f \Rightarrow R_o = \sqrt{\frac{A_o^y}{\pi}} = \sqrt{\frac{350 \times A_o^f}{\pi}}. \tag{74}$$

We recall that $A_o^c = \pi((R_o + \mathcal{T})^2 - R_o^2)$, which is an effective coating area. Since a single yarn does not take the entire load, the absorbed (stored) energy and the mass of the yarn are multiplied (see Equations 63 and 64) by the number of yarn, Y ("load sharers" Figure 7) to compute the effective inertia and effective absorbed (stored) energy, yielding

$$i^* = \frac{ln\gamma_e}{ln\alpha_e}, \tag{75}$$

where

$$\gamma_e = \frac{\frac{-\beta_e}{\alpha_e}}{(\alpha_e - 1)(v_p^{(0)})^2 - \beta_e}, \tag{76}$$

and

$$\alpha_e = \frac{m_p}{m_p + \frac{Y(\rho_o^y A_o^y L_o + \rho_o^c A_o^c L_o)}{3}} \quad \text{and} \quad \beta_e = \frac{2Y(w^y(U^{*,y}) + w^c(U^{*,c}))}{m_p + \frac{Y(\rho_o^y A_o^y L_o + \rho_o^c A_o^c L_o)}{3}}. \quad (77)$$

The typical denier (yarn weave density) of a Zylon weave is 35 yarn/inch (=$35 \times (100/2.54) = 3500/2.54 \approx 1378$ yarn/meter). In order to estimate the number of yarn that share the load in a sheet, for a cylindrical penetrator, such as the one used in the experiments, we took twice the diameter (yarn in the vertical and horizontal directions) of the projectile (0.0127 meters) and multiplied this by the yarn per unit length (Figure 7). Thus, the number of yarn that share the load is approximately $2 \times 0.0127 \times 35 \times (100/2.54) = 35$ and the number of fibrils is approximately $350 \times 35 = 12250$. Inserting this data into Equation 75 yields $i^* = 6.52$, which asserts that approximately seven sheets (conservatively rounding up to an integer value) will be penetrated by the projectile and that eight $(i^* + 1)$ sheets are needed to stop the projectile. The laboratory experiments described earlier in the introduction indicated that, for a projectile initially traveling at approximately 350 feet/sec (106.68 meters/sec) penetrated six (boundary) clamped sheets. Therefore, seven sheets were needed to stop the projectile. One key reason for the close agreement between the analytical and experiment results is the choice of the linear velocity profile in the fully deformed configuration, which essentially matches the observed state of the fabric for clamped boundary conditions. Essentially only the yarn shown in Figure 7 participate to any significant degree in the ballistic resistance for clamped boundary conditions. Figure 8 illustrates the typical velocity/sheet-penetration square-root (sub-linear) behavior widely observed in ballistics studies. The $v_o = 300\,m/s$ case has approximately nine times the initial kinetic energy as the $v_o = 106\,m/s$ case, thus leading to approximately nine times the sheets needed.

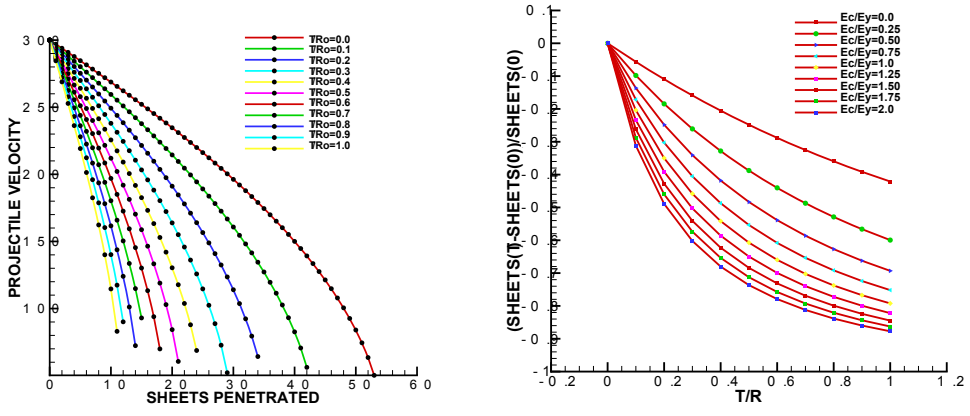

Fig. 8 (online colour at: www.gamm-mitteilungen.org) LEFT: For $v_o = 300\,m/s$-coating variation of $\mathcal{T}/R_o = 0, 0.1, 0.2 \ldots 1$. The $v_o = 300 m/s$ case has approximately nine times the initial kinetic energy as the $v_o = 106 m/s$ case, thus leading to approximately nine times the sheets needed. RIGHT: $v_o = 300 m/s$: Trends for increasing coating stiffness, $\mathbb{E}^c$, in increments of $0.25 \times \mathbb{E}^y$, starting from $\mathbb{E}^c/\mathbb{E}^y = 0$ (top curve) to $\mathbb{E}^c/\mathbb{E}^y = 2$ (bottom curve). Note the coating density used was $\rho^c = 5000 kg/m^3$.

Of primary interest is to plot the reduction of the number of sheets needed to stop the projectile, $I^*(\mathcal{T}) \stackrel{\text{def}}{=} \frac{i^*(\mathcal{T})-i^*(0)}{i^*(0)}$, as a function of the coating thickness, where $i^*(\mathcal{T})$ is the number of sheets needed with added coating of thickness $(\mathcal{T})$ and $i^*(0)$ is the number of sheets needed with no coating. In Figure 8, the trends are illustrated for an incoming projectile velocity of $v_o = 300m/s$, with curves for increasing coating stiffness, $\mathbb{E}^c$, in increments of $0.25 \times \mathbb{E}^y$, starting from $\mathbb{E}^c = 0 \times \mathbb{E}^y$ (top curves/not stiff coatings) to $\mathbb{E}^c = 2 \times \mathbb{E}^y$ (bottom curves/stiff coatings). A coating density of $\rho^c = 5000kg/m^3$ was used.[15] There is a mild reduction of the number of sheets needed for soft coatings ($\mathbb{E}^c << \mathbb{E}^y$), which is attributable to the increased mass of the sheets. For weak (not stiff) coatings, this trend has a nearly linear dependence on $\mathcal{T}/R_o$. However, for sufficiently stiff coatings, the curves illustrate the dramatic (essentially exponential) reduction of the number of sheets needed to stop the projectile. The utility of this analysis is that the analytical expression/curves provide a quick way to *qualitatively* study the decrease in sheets needed as a function of added mass (or, alternatively, coating thickness). *However, clearly, the model has utility to describe qualitative effects, but is deficient in dealing with projectiles with a non-flat profile, where the contact area changes as well as frictional sliding between the projectile and fabric.* However, the model can serve as a building block to construct a computational framework for networks of coated yarn which form sheets. This is discussed in the main body of the paper.

[15] In addition, we used the same critical stretch parameter for the fabric and coating ($U^{*,c} = U^{*,y}$).

